ELSEVIER

Contents lists available at ScienceDirect

Chemical Engineering Journal

journal homepage: www.elsevier.com/locate/cej





A modelling workflow for quantification of photobioreactor performance

Wenjia Gu^a, Emile Theau^a, Amos W. Anderson^b, David F. Fletcher^a, John M. Kavanagh^a, Dale D. McClure^{a,c,*}

- ^a School of Chemical and Biomolecular Engineering, The University of Sydney, 2006, Australia
- ^b School of Life and Environmental Sciences, The University of Sydney, Sydney, NSW 2006, Australia
- c Department of Chemical Engineering, College of Engineering, Design and Physical Sciences, Brunel University, London, Uxbridge UB8 3PH, UK

ARTICLE INFO

Keywords: Photobioreactor Scale-up CFD Microalgae Particle tracking

ABSTRACT

In this work we have developed a comprehensive modelling workflow for the quantification of photobioreactor performance. Computational Fluid Dynamics (CFD) modelling combined with Lagrangian particle tracking was used to characterise the flow field inside the reactor; this information was combined with a Monte-Carlo model of light attenuation and a kinetic growth model to predict the performance of the system over the duration of the entire batch. The CFD model was validated against measurements of the overall hold-up, local hold-up and mixing time for superficial velocities between 0.6 and 6 cm s⁻¹ in a pilot-scale bubble column photobioreactor, with the CFD predictions agreeing with the experimental data. Comparison was also made between the predicted biomass concentration and experimental measurements using the diatom *Phaeodactylum tricornutum*, with the model predictions being in good agreement with the experimental results. The model was used to investigate a range of operating conditions and reactor designs, with the most promising predicted to give a 40 % increase in the biomass productivity. Results from this work can be used for the *in-silico* design and optimisation of photobioreactor systems, thereby enabling their wider use as a sustainable production technology.

1. Introduction

Photoautotrophic microorganisms (e.g., microalgae and cyanobacteria) can be used for the sustainable production of a range of compounds including high-value products for the food industry (e.g., carotenoid pigments, omega-3 fatty acids, vitamins) [1], biofuels [2] and chemicals [3]. A major advantage of using photoautotrophic microorganisms is their minimal nutrient requirements; light and carbon dioxide are the primary feedstocks. This may be advantageous from a sustainability perspective as there is no need for arable land, potable water and also no competition with food crops [4]. A major challenge in the commercialization of bioprocesses using photoautotrophic microorganisms is the process economics [1]. The majority of existing processes utilize open photobioreactors (e.g., ponds and raceways), which have the advantage of lower capital costs than closed systems (e.g., flatpanel, bubble column and tubular photobioreactors) [1]. However, open photobioreactors are susceptible to contamination and may not be appropriate for all organisms (e.g., it may not be suitable to grow engineered organisms in an open system).

Closed photobioreactors can generally achieve higher cell densities and biomass productivities than open systems, and are less susceptible to contamination [5]. The major challenge with such reactors is efficiently using the available light to achieve high cell densities. As the distance from the illuminated surface of the Photo Bio Reactor (PBR) increases the light intensity decreases in an exponential fashion due to absorption and scattering of light by the cells [6]. This can lead to a situation where the central volume of the reactor is essentially 'dark', with the cells located in this volume receiving insufficient light for photosynthesis. Under conditions of high illumination (e.g., near the walls of the reactor) the capacity of the electron transport chain (the biochemical pathway involved in absorbing energy from light) can become saturated, which can lead to the production of reactive oxygen species and in turn damage to the cells [7]. In practice, cells will alternate between zones of high and low light intensity due to transport by the liquid. The extent to which this occurs will depend on the reactor design and operating conditions [8,9]. By optimizing the frequency at which cells move between zones of light and dark it may be possible to improve the utilization of the incident light (the flashing light effect). Numerous authors [10-15] have examined this problem, reporting that light-dark frequencies of the

E-mail address: dale.mcclure@brunel.ac.uk (D.D. McClure).

^{*} Corresponding author at: Department of Chemical Engineering, College of Engineering, Design and Physical Sciences, Brunel University, London, Uxbridge UB8 3PH. UK.

Nomenclature		p	[-], Number of cells
		P	[-], Random number
Symbol	Units, Description	R	[m], Photobioreactor radius
F	[s ⁻¹], Light/dark cycle frequency	x	[m], Distance in x direction
g	[-], Scattering constant	\boldsymbol{X}	[kg m $^{-3}$], Cell density
H_L	[m], Liquid height	y	[m], Distance in y direction
H_{G+L}	[m], Height of two-phase mixture	z	[m], Distance in z direction
I	[μ mol photons m ⁻² s ⁻¹], Light intensity	α	[-], Gas volume fraction
I_0	[μ mol photons m ⁻² s ⁻¹], Initial light intensity	Γ_{max}	[-], Constant in growth model
I_n	[μ mol photons m ⁻² s ⁻¹], Light intensity at point n for a	Δl	[m], Propagation distance of photon
	photon	θ	[radians], Scattering angle for photon
\overline{I}_p	[μ mol photons m ⁻² s ⁻¹], Time-averaged light intensity for	μ	[s ⁻¹], Specific growth rate
•	photon p	$\overline{\mu}$	[s ⁻¹], Population-averaged specific growth rate
k	[-], Constant in growth model	μ_{full}	[s ⁻¹], Specific growth rate with full light integration
K_{a}	[m ² kg ⁻¹], Attenuation constant	$\mu_{ m max}$	[s ⁻¹], Maximum specific growth rate
K_F	[s ⁻¹], Constant in growth model	$\mu_{ m no}$	[s ⁻¹], Specific growth rate with no light integration
K_I	[μ mol photons m ⁻² s ⁻¹], Half saturation constant	ρ_G	[kg m $^{-3}$], Gas density
n	[-], Constant in volume fraction correction term model	ρ_L	$[kg m^{-3}]$, Liquid density
$n_{ m total}$	[-], Total number of time points used in averaging	σ	[kg s $^{-2}$], Surface tension
	procedure		

order 10–100 Hz are needed to make maximum use of the flashing light effect [11,12,16], while some benefits may be obtained at frequencies of the order 0.08 Hz [17]. Understanding the light intensity experienced by cells within a PBR, the light–dark cycle frequency and how these variables are affected by the reactor design and operating conditions is key in PBR design and optimization.

As previously noted, a major challenge in PBR design is making effective use of the supplied light to achieve high cell densities. One way in which this can be achieved is to simply reduce the thickness of the reactor, thereby reducing the optical path length and hence the amount of light attenuation. However, this has the significant drawback of requiring a higher surface area for the same liquid volume, thereby increasing the capital cost. Another potentially promising direction is the use of internal structures (e.g., baffles, static mixers, etc.) which promote mixing within a PBR and hence potentially increase the light--dark cycle frequency. It is hypothesized that by promoting mixing between the central 'dark' region of the PBR and the illuminated wall region cells will experience higher light intensities and this in turn will lead to higher cell densities. Recent work has found this to be the case, for example installation of baffles was found to increase the biomass productivity of Chlorella cultures by 60-90 % [18-22]. Similarly, Ryu et al. demonstrated that the use of horizontal sieve baffles and slanted baffles led to approximately 40 % increases in the biomass concentration of Chlorella sp. in 4 cm diameter cylindrical bubble column PBRs [23]. Merchuk et al. showed that the installation of helical flow promoter in cylindrical PBRs lowered the air flow rate required to achieve the maximum cell density of Porphyridium sp. cultures and thereby reduced the energy expenditure in air compression [24]. Such results demonstrate the potential of modified reactor designs, while also highlighting the need for tools to better understand the hydrodynamics of PBRs in order to facilitate the development of optimised reactor designs.

Computational Fluid Dynamics (CFD) models are increasingly [25] being used as tools to model bioprocesses, including photobioreactors [26–30]. In the case of photobioreactors Lagrangian particle tracking is a particularly useful approach [31]. Particles having the same density and size as cells are included in the model which tracks their position in the reactor as a function of time. Using this information it is possible to construct the 'history' or 'lifeline' of a given cell as it moves throughout the reactor. As the light intensity experienced by a cell is largely a function of its location it is possible to determine the light intensity experienced by a cell as a function of time by coupling the particle tracking approach with a model of light attenuation. From this it is

possible to then determine key information like the light—dark cycle frequency and the average light intensity. By including a large number of cells in the model it is also possible to calculate population-averaged values. Such an approach based on Lagrangian particle tracking has the advantage that it is likely to be the most representative of the behavior occurring within the photobioreactor, and as such may offer the most accurate way of quantifying reactor performance.

CFD models have the advantages of providing a high degree of spatial and temporal resolution, and allowing for multiple reactor configurations to be evaluated in silico, thereby minimizing the need for experimental work. Another key advantage is that models can be used to generate information which is very difficult to obtain experimentally (e. g., simulating the movement of cells throughout a PBR). A disadvantage of CFD models is that their high computational demand means that it is only feasible to simulate a relatively short length of time (typically hundreds of seconds), while a typical growth cycle in a PBR would last several days/weeks. Hence, it is not possible to use CFD to simulate an algal cultivation from start to finish. To circumvent this limitation, results from simulations of the fluid dynamics can be combined with light and growth models to give an overall model which can predict the overall process performance [32,33]. Such models can be used to understand the reactor performance and develop optimized designs; however, relatively little work has been done in this area looking at bubble column photobioreactors.

Use of a CFD model to quantify the performance of PBRs obviously relies on having accurate predictions of the hydrodynamics in order to correctly predict the trajectory of the cells. Hence, before any CFD model can be used to quantify the performance of the PBR it should be validated against experimental data to ensure it offers accurate predictions of the hydrodynamics. Our previous work [34,35] has focused largely on the modelling of large-scale aerobic bioprocesses, which typically operate at higher superficial velocities (>0.1 m s $^{-1}$) than PBRs (which typically operate at superficial velocities below 0.05 m s $^{-1}$). Therefore, before the model can be used as a tool to quantify PBR performance there is a need to validate its predictions at conditions found in PBRs.

The aim of this work is to develop and validate a modelling workflow which can be used to quantify the effect of PBR design and operating conditions on performance, and to use such a model to identify improved reactor designs. To do this it is firstly necessary to validate the CFD methodology used, and secondly to integrate the CFD model with models of light attenuation and growth and determine whether the combined workflow provides accurate predictions of algal growth. Once

the modelling workflow has been validated it can then be used as a tool to examine different designs with the aim of identifying those which will provide improved performance.

2. Method

2.1. Experimental measurements

Experimental measurements used to validate the CFD model were performed using the bubble column configuration without any internals. The bubble column used in this work was 190 mm in diameter, 2000 mm in height and it was fabricated from clear acrylic. Air was introduced

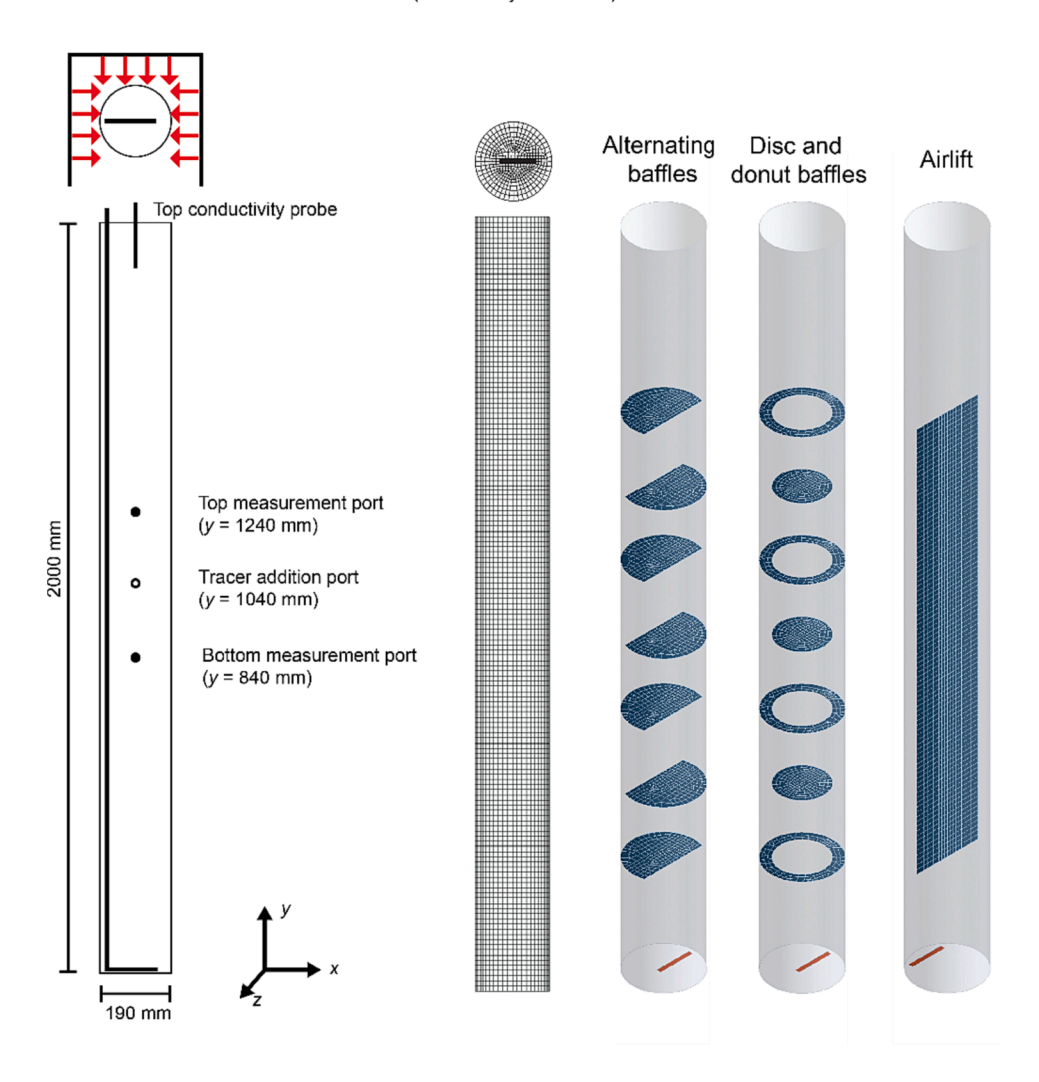
through an L-shaped stainless-steel perforated tube sparger. The sparger had three rows of 10×2 mm diameter holes. There was a 10 mm spacing between hole centres. A detailed schematic of the sparger is shown in Fig. 1.

Compressed air was sourced from the building supply. The flow rate was measured using a RM series rotameter (Dwyer) and corrected to the flow rate at standard conditions (298 K and 101325 Pa) using measurements of the pressure at the rotameter outlet (typically 14–17 kPa as measured using a Dwyer LPG3 series pressure gauge). Volumetric flow rates were converted to the superficial velocity by dividing the flow rate at standard conditions by the cross-sectional area of the column.

Measurements of the liquid height (H_L) and the height of the two-

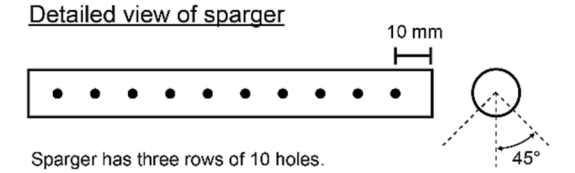
Top view of column

The column is illuminated from three sides (indicated by red arrows)





Photograph showing column with growth of P. tricornutum



The middle row faces downwards. The centre of the other two rows is \pm 45° from the centreline of the middle row. The rows have 10 mm spacing between hole centres.

Fig. 1. Schematic of bubble column photo-bioreactor, as well as the mesh used in the CFD modelling.

phase mixture (H_{G+L}) were made using a ruler attached to the side of the column and these values were used to calculate the overall hold-up (α):

$$\alpha = 1 - \frac{H_L}{H_{G+L}} \tag{1}$$

Three measurements of the hold-up were made at each superficial velocity. Reported results are the average of these three measurements. Error bars denote one standard deviation about the mean or the error as calculated using error propagation methodology, whichever was larger.

The bubble size distribution (BSD) was measured using two-point needle probes, details of the probe design are described in detail elsewhere [36]. The measured chord-length distribution was converted to the BSD using the non-parametric transform developed by Liu et al. [37], here it was assumed that the bubbles were ellipsoidal in shape with a fixed aspect ratio of 0.6. Probes were positioned on the column centerline, facing down at heights of 800 and 1200 mm above the base of the column. Measurements of the BSD were made at superficial velocities of 0.6, 1.6, 3.2 and 6.0 cm s $^{-1}$. Three measurements each 180 s in duration were made at each condition, these data were combined for analysis. The error in the reported mean bubble sizes is of the order \pm 20 %, as determined in our previous work [36].

Local hold-up measurements were made using single-point needle probes as detailed elsewhere [36]. Probes were located at heights of 840 and 1240 mm above the base of the column and at radial locations of 0, \pm 30, \pm 60 and 90 mm. Measurements made at a location of - 90 mm generally did not result in a signal, most likely due to the small (5 mm) gap between the column wall and the probe tip (meaning no bubbles were able to pass through the gap), similar behavior being observed in our previous work [38]. The local volume fraction was measured for 5 \times 30 s at each point, with reported values being the average, error bars denote one standard deviation about the mean. It was found that areaaveraging the local hold-up profiles gave overall hold-up values less than the experimentally measured overall hold-up value, suggesting that some bubbles were 'missed' by the probes. To correct for this the measured values were multiplied by the ratio between the overall holdup and the area-averaged local hold-up, this being 1.35 for measurements at a height of 1240 mm above the base of the column and 1.65 for measurements made at a height of 840 mm above the base of the column. The same correction factor was used for all superficial velocities examined.

Mixing in the column was quantified by measuring the mixing time. This was measured by adding a salt tracer (4 M NaCl) and measuring the conductivity as a function of time. Conductivity probes (Real Time Instruments) were positioned at heights of 840, 1240 and 1700 mm above the base of the column, as shown in Fig. 1. The probes located in the middle of the column were positioned at the centerline. To quantify the effect of the tracer addition location it was added both to the top of the column (by pouring on to the free surface) or by injecting it into a port 1040 mm above the base of the column. A volume of 130-150 mL of tracer was used. All measurements were made in triplicate, the reported values are the average with error bars denoting one standard deviation about the mean. This approach was used in order to quantify the variability in the mixing time caused by the inherently transient nature of flow inside bubble columns. After three tracer additions the column was drained and refilled to minimize the effect of salt addition on the hydrodynamics. The mixing time was defined as the time required for the tracer concentration to settle within \pm 5 % of the final equilibrium value. Further details about the methodology used are presented elsewhere [39].

2.2. CFD modelling

In this work we have applied a computational approach we developed previously and validated for bubble columns [38,40]. In this work the Euler-Euler approach is used to model the two-phase flow. Inter-

phase momentum transfer is modelled as the sum of drag and turbulent dispersion. The drag force was calculated using the Grace et al. model for an isolated bubble [41], combined with a volume fraction correction term based on our previous work [42], values of the constants n and b were 50 and 0.20, respectively. Bubbles had a fixed size (8 mm), this being the experimentally measured mean value (see Supplementary Fig. S6). Turbulent dispersion was modelled using the Favre-averaged drag approach outlined by Burns et al. [43]. Liquid phase turbulence was modelled using the standard k- ε approach as implemented in Ansys CFX, with the source terms developed by Yao and Morel [44] being included to account for bubble-induced turbulence. Gas-phase turbulence was modelled using the dispersed phase zero approach. This approach was used as it has been shown to provide good agreement with experimental data across a broad range of column designs and operating conditions [34,40].

A schematic of the mesh used is shown in Fig. 1, a hexahedral mesh with 58,800 elements was used. To ensure the model predictions were independent of the grid size simulations were also performed with coarse (36,120 elements) and fine (132,480 elements) meshes. As shown in Supplementary Fig. S1 it was found that the results did not depend on the grid size used.

The sparger was modelled as an inlet boundary condition on the bottom face of the column 12.5 mm in width and 90 mm in length. The top of the column was modelled as an outlet at atmospheric pressure, the remaining surfaces, including the column walls and any internals, were modelled as walls using the no-slip condition for the liquid and free-slip for the gas. Baffles were spaced 200 mm apart, with the bottom baffle being 300 mm from the base of the column. The alternating baffles were 125 mm wide, the disc shaped baffles had a diameter of 134 mm, while the cut-out in the donut baffles was also 134 mm. The baffle for the airlift was located on the column centerline 300 mm above the base of the column, the height of the baffle was 1200 mm.

An initial liquid height of 1.70 m was used, below this height the liquid volume fraction was one, while above it the initial liquid volume fraction was zero (i.e. the headspace was full of gas as is physically correct). Densities of 1.2 kg m $^{-3}$ and 1000 kg m $^{-3}$ were used for the gas and liquid phases respectively. A value of 0.072 N m $^{-1}$ was used for the surface tension. The viscosities of the gas and liquid phases were 1.83 \times 10^{-5} Pa s and 1×10^{-3} Pa s, respectively.

Ansys CFX 2021R1 was used in this work. The bubble column flow was modelled as a transient using small timesteps $(1 \times 10^{-3} \text{ s})$ as is required for such two-phase flows. Each simulation was run for a period of 150 s before averaging, then for an additional 150 s with transient averaging turned on. Unless stated otherwise all reported results are transient averages. All runs were solved using double-precision and further details about the numerical methods used are available elsewhere [40].

In order to quantify the predicted mixing time tracers were introduced at the same locations as those used experimentally (see Fig. 1). Tracers were introduced at 151, 161 and 171 s, this being done to account for any fluctuations in the hydrodynamics which is known [39] to affect the mixing time. The tracer concentration was calculated at the same locations as used experimentally, and like the experimental results the reported values are the average of the three repeats, with error bars denoting one standard deviation about the mean.

2.3. Coupling of CFD with algal growth kinetics

In this work, we have developed an approach that integrates CFD particle tracking with algal growth kinetics, thereby allowing simulation of the influence of flashing light on biomass accumulation over time. The workflow used for the model integration is shown in Fig. 2.

To understand the distribution of algal cells throughout the reactor 2,000 Lagrangian particles were introduced at one timestep (i.e. 1×10^{-3} s) at a simulation time of either 150 or 300 s, with their location in the column being tracked for 150 s. The particles (representing cells)

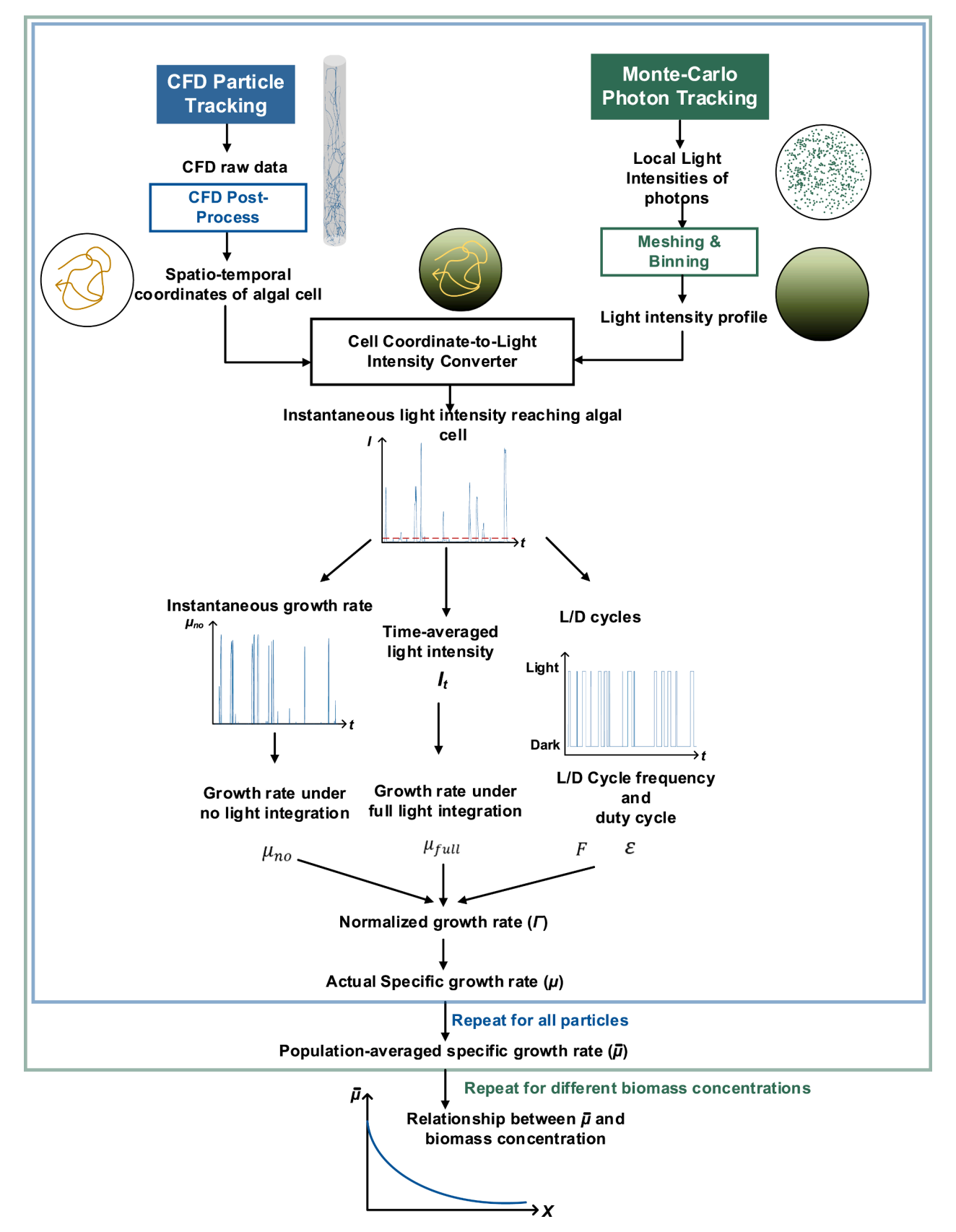


Fig. 2. Schematic showing the workflow used in the model.

were introduced uniformly throughout the column, using a grid with 20 \times 10 evenly spaced particles with 10 radial divisions. The particle post-processing was done using a custom script written in Matlab R2022. The particle solver in Ansys CFX uses a variable time-step [45]. To simplify the analysis an array having a fixed timestep (0.01 s) was generated and the particle x and z coordinates generated by the CFD model were interpolated onto this array using the one-dimensional spline interpolation function implemented in Matlab R2022. Any particle where the track ended before the designated time (150 s) was excluded from the analysis; this corresponded to a maximum of 3.6 % of the particles added.

The distribution of local light intensity within the PBR was simulated by adopting a Monte Carlo type procedure that tracks the trajectories of numerous photons within the PBR, following the method developed by others [32]. This approach accounts for absorption of light, as well as changes in the trajectories of the photons due to scattering. Here it was assumed that the light intensity was uniform in the vertical (y) direction, meaning light attenuation was only modelled in two-dimensions (i.e., along the x and z coordinates). Other optical phenomena, such as the refraction and reflection across/by the PBR wall were omitted. When modelling the configurations with internals (i.e., the bubble column with segmented baffles, disc and donut baffles and the airlift) any effect of the internals on the light propagation was neglected. Additionally, it was assumed that the cells were distributed uniformly throughout the medium, and the effects of the bubbles on the light scattering were minimal (in line with results reported elsewhere [28]). No wavelength dependent behaviour was considered in this work. Furthermore, it was also assumed that the hydrodynamic behavior did not change throughout the course of a batch, something which is likely to be true provided the algae do not produce large quantities of extracellular compounds which could affect the fluid flow. Hence, the same CFD results were used to represent the hydrodynamics (using the Lagrangian particle tracks) for the entirety of the batch.

In modelling the trajectory of a photon, the photon enters the PBR from one of the illuminated surfaces of the PBR, each of which covered a 180° arc. The photon propagates through the medium for a distance, Δl , before it is scattered, this scattering changes its direction. The photon then travels for another distance (Δl) before being scattered again. This procedure continues until the photon exits the boundary of the PBR, or its intensity reaches a value of $0.1~\mu mol$ photons $m^{-2}~s^{-1}$, at which point the tracking process was stopped. The position of a photon at step n is determined based on its position at the previous step (n-1):

$$x_n = x_{n-1} + \Delta l \bullet \cos\theta \tag{2}$$

$$z_n = z_{n-1} + \Delta l \bullet \sin\theta \tag{3}$$

The Monte Carlo sampling procedure was used to determine (a) the starting position of a photon, (b) the propagation distance (Δl) at each step and (c) the scattering angle (θ) at each step.

As shown in Fig. 1, the PBR is illuminated by three light sources; each covered 180° of the PBR surface. In determining the starting position of a photon, a value was sampled from a uniform distribution across the interval $[0, \pi]$, and the distance to the PBR centre was one PBR radius (R). At this starting position, the photon has an incident intensity (I_0) of $360 \,\mu\text{mol}$ photons m⁻² s⁻¹, this being the experimentally measured light intensity on the side of the photobioreactor [46].

The propagation distance for the photons (Δl) was set to be a random number across the uniform distribution between 0 and 1 mm. The scattering angle (θ) was determined using the Henyey-Greenstein phase function [32]:

$$\cos(\theta) = \frac{1}{2g} \left\{ 1 + g^2 - \left(\frac{1 - g^2}{1 + g(2P - 1)} \right)^2 \right\}$$
 (4)

where P is a random number drawn from the uniform distribution be-

tween 0 and 1. The amount of forward and back-scattering is adjusted by the value of the parameter g, with g=1 corresponding for forward scattering only, and g=0 corresponding to isotropic scattering. Here a value of g=0.95 was used, this being based on the experimental work of Marken et al. [47].

The attenuation in the light intensity between two consecutive steps due to absorption was accounted for using the Beer-Lambert equation. The local light intensity at each step (I_n) was expressed as:

$$I_n = I_{n-1}e^{-K_a X \Delta l} \tag{5}$$

where K_a is the attenuation constant. Here we have used a value of $0.35 \, \mathrm{L \ mg^{-1} \ m^{-1}}$ for the light attenuation constant (K_a) , this value being based on our previous work [46]. I_{n-1} is the local light intensity at the previous step; Δl , is the propagation distance in this step; X is the biomass concentration.

The output of the Monte-Carlo procedure was an array containing the position and intensity of photons throughout the photobioreactor for each of the light sources. To enable use of these data to generate a light profile across the PBR, the horizontal (XZ) plane of the PBR was discretized onto a two-dimensional mesh containing 6078 elements, this was generated using the Delaunay triangulation methodology implemented in Matlab. Photons were allocated to a mesh element based on their x, z coordinates. The light intensity in each mesh element for a given light source was calculated by averaging the intensity of all photons allocated to that element. From this the total light intensity was determined by taking the sum of the light intensity from each of the three sources. This procedure generated a two-dimensional map of the light intensity (see Fig. 7). Using these data, it was possible to allocate the particles from the CFD model to a mesh element at each time point (based on their x, z coordinates) and hence generate an array containing the light intensity for each timepoint for each particle.

The growth rates of the cells under flashing light were determined following the findings by Terry for *P. tricornutum* [10]. At very high L/D cycle frequencies (i.e., those much greater than 1 Hz) the cells are thought to respond as though the lighting is continuous, and hence the growth rate (μ_{full}) can be calculated based on the time-averaged light intensity for the particle (\bar{I}_p) [10]:

$$\mu_{\text{full}} = \frac{\mu_{\text{max}} \overline{I}_p^{\ k}}{\overline{I}_p^{\ k} + K_I^{\ k}} \tag{6}$$

where the $\mu_{\rm max}$ is the maximum specific growth rate (2.4 day⁻¹), K_I is the half-saturation constant for light (50 μ mol photons m⁻² s⁻¹) and k is a constant (1.9). Values of the constants in the growth model are based on our previous experimental work and that of others in the literature [46,48]. The time-averaged light intensity for each particle \bar{I}_p was calculated using the interpolated values:

$$\bar{I}_p = \frac{\sum_{n=1}^{n_{\text{total}}} I_{p,n}}{n_{\text{total}}} \tag{7}$$

where $I_{p,n}$ is the instantaneous light intensity experienced by particle p at time n and n_{total} is the total number of time points (here 15,000).

At sufficiently low L/D cycle frequencies the growth rate of the cell depends on the instantaneous light intensity experienced by the particle (I_p) meaning there is no light integration. This can be used to calculate the specific growth rate:

$$\mu_{\rm no} = \frac{\mu_{\rm max} I_p{}^k}{I_p{}^k + K_I{}^k} \tag{8}$$

Partial light integration will occur at L/D cycle frequencies between those where full and no light integration occurs; these are the frequencies likely to be found in industrial photobioreactors. Here the specific growth rate depends on the L/D cycle frequency (F):

$$\mu = \frac{\Gamma_{\text{max}} F}{K_{\text{r}} + F} \left(\mu_{\text{full}} - \mu_{\text{no}} \right) + \mu_{\text{no}} \tag{9}$$

where Γ_{max} and K_F are constants; Terry [10] determined that the values of Γ_{max} and K_F to be 0.972 and 0.67 Hz, respectively, for *P. tricornutum*.

Here we have defined a cell as being in the dark if the instantaneous light intensity was less than 5 μ mol photons m⁻² s⁻¹. This value was selected on the basis that at this light intensity the net growth rate is zero (i.e., the light intensity is sufficient for cellular maintenance but not growth) [49]. Using the calculated values of the instantaneous light intensity it is possible to determine whether or not a particle is in the light or dark zone for each time point. From this it is possible to determine the L/D cycle frequency and thus the specific growth rate (μ) for this cell. The specific growth rate was determined for each of the simulated algal cells; the mean of the specific growth rates of the cell population was then calculated:

$$\overline{\mu} = \frac{1}{p} \sum_{i=1}^{p} \mu_i \tag{10}$$

where p is the number of cells evaluated.

The Monte Carlo sampling procedure and the subsequent determination of the growth rate for the algal cell population were repeated for biomass concentrations ranging between 5 and 2005 mg L $^{-1}$, thereby generating a set of datapoints providing the population averaged specific growth rate ($\overline{\mu}$) for the range of cell densities examined. These data were integrated with our recently developed, ODE-based model for simulating the growth of the alga *P. tricornutum* [46]. Here, it was assumed that light was the sole growth-limiting factor. In the model the specific growth rate for a given cell density was found by interpolating onto the $[X, \overline{\mu}]$ array generated using the workflow developed in this paper. The one-dimensional spline interpolation function implemented in Matlab R2022 was used to perform the interpolation.

To ensure the results were independent of the numerical values used in setting up the simulation a range of conditions were investigated, with the full details being available in the Supplementary Material. Simulations were performed to investigate the effect of the number of photons per light source (100, 300, 500, 1000 and 10,000), the number of mesh elements (570, 1710, 6078 and 14,286) and the number of Lagrangian particles (200, 500, 1000 and 2000). Based on these results all subsequent simulations were performed with 1000 photons per light source, a mesh containing 6078 elements and 1000 Lagrangian particles.

2.4. Algal cultivation experiments

In this work we have focused on the cultivation of *Phaeodactylum tricornutum*, a marine diatom which can be used for the production of valuable compounds like eicosapentaenoic acid and fucoxanthin [50–52]. Cultivations were performed using the bubble column configuration as described in Section 2.1. Air (supplemented with 1 % (v/v) carbon dioxide) was introduced into the column at a superficial velocity of 1.3 cm s $^{-1}$. Here 1 % (v/v) carbon dioxide was used as this concentration is sufficient to maintain the pH below 8.5, hence ensuring the growth is not limited by the availability of carbon.

Cultures were illuminated for 16 h per day using the LED lights mounted on three sides of the column (Fig. 1). The lighting consisted of 9 W cool-white (6000 K color temperature) LED bars (Jaycar Australia), these were arranged in a 3×5 grid (vertical \times horizontal) on each of the illuminated sides of the PBR. To quantify the biomass density samples (typically 50–60 mL) were taken and filtered using pre-weighed glass fibre filters (Advantec GA-55, Toyo Roshi Kaisha Ltd, Tokyo Japan). Samples were washed with three volumes of 0.5 M ammonium bicarbonate before being dried at 105 $^{\circ}\text{C}$ overnight. After drying the samples were cooled and then weighed to determine the dry cell weight. Further details about the cultivation conditions and the analytical methods are available in our previous work [46].

3. Results and discussion

3.1. CFD model validation

As the performance of the model relies upon accurate predictions of the hydrodynamics within the reactor it is necessary to validate the CFD model against experimental data. Fig. 3 gives a comparison between the experimentally measured overall hold-up values and those predicted by the CFD model, while a more detailed comparison of the local-hold-up profiles is given in Fig. 4. It was found that there was good agreement between the experimental measurements and the model predictions, with the model slightly under-predicting the hold-up. Interestingly the maximum values for the experimentally measured hold-up values were found to occur at x = 30 mm and not at the column centerline (as was found for the CFD predictions). Such results could be because the CFD model over-predicts the extent to which the bubble plume becomes symmetrical. This could be caused by the model over-predicting the magnitude of the turbulent dispersion force, or over-predicting the eddy viscosity which would damp out oscillations. Equally such results could be due to the fact that the sparger is not located perfectly perpendicular to the measurement location, thereby introducing a degree of asymmetry into the results. While every attempt was made to ensure that the sparger was located on the centerline of the column it was possible that it could have moved by a small amount (of the order 10 mm). Interestingly, it appears that at higher superficial velocities the observed asymmetry is reduced (Fig. 4 (h)). Inclusion of the lift force, or modification of the coefficient in the turbulent dispersion model may lead to improved agreement with the experimentally measured hold-up profiles. However, this was not pursued as the model gives reasonable agreement with the overall and local hold-up, as well as the mixing time (Fig. 5).

Experimentally measured bubble size distributions are shown in Fig. S6 in the supplementary data. It was found that the superficial velocity had a relatively small effect on the bubble size distribution, while the distance from the sparger had a larger effect. Measured mean bubble sizes were of the order 10–12 mm at a height of 800 mm above the base of the column and 8–9 mm for a height of 1200 mm above the base of the column. The correlation developed by Akita and Yoshida [53] predicts

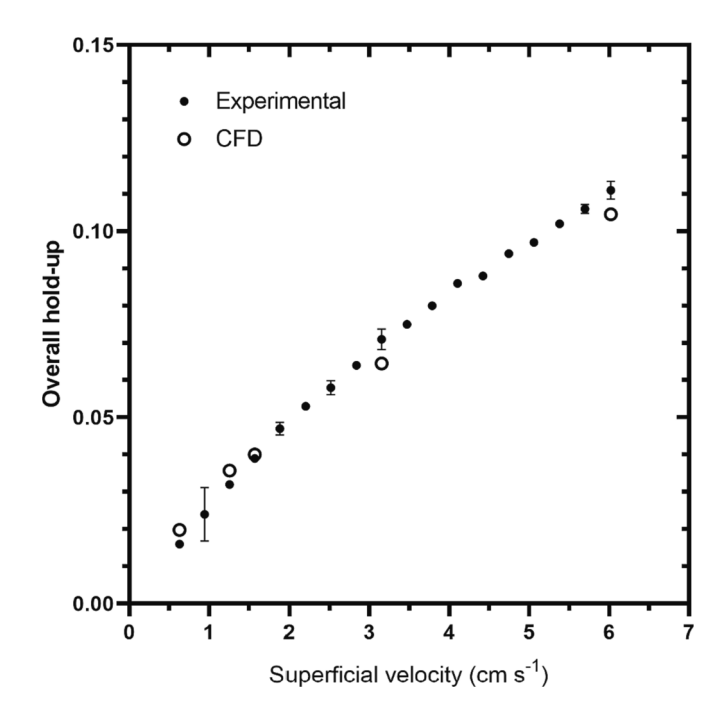


Fig. 3. Plot showing comparison between experimentally measured overall hold-up values and those predicted by the CFD model.

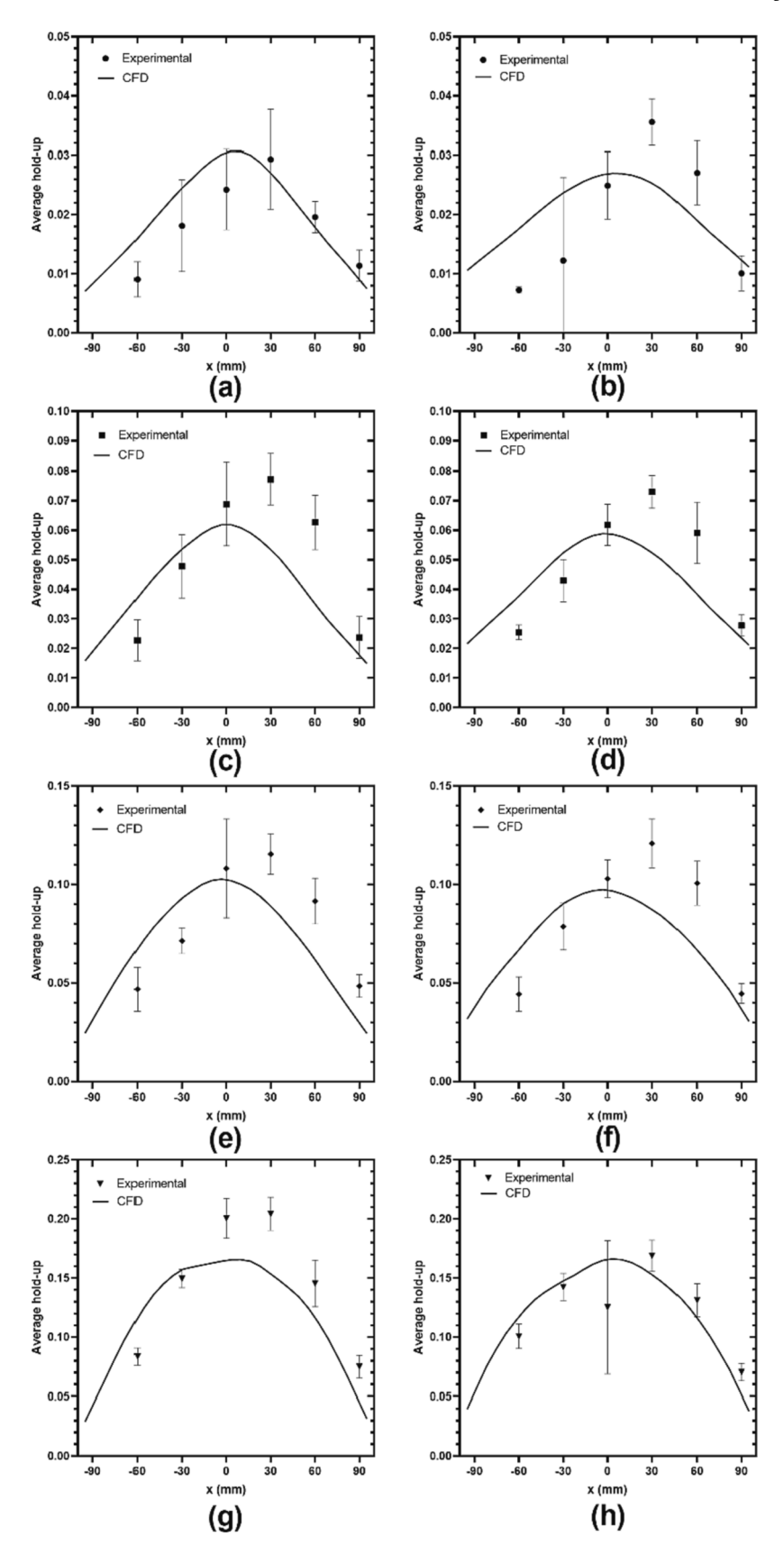


Fig. 4. Plot showing comparison between experimentally measured local hold-up profiles and those predicted by the CFD model. Results on the first row (a) and (b) are for a superficial velocity of 0.6 cm s^{-1} , those on the second row (c) and (d) are for a superficial velocity of 1.6 cm s^{-1} , those on the third row (e) and (f) are for a superficial velocity of 3.2 cm s^{-1} and those on the final row (g) and (h) are for a superficial velocity of 6.0 cm s^{-1} . Plots in the first column (a), (c), (e) and (g) are for a height of 840 mm above the base of the column, while those in the second column, (b), (d), (f) and (h) are for a height of 1240 mm above the base of the column.

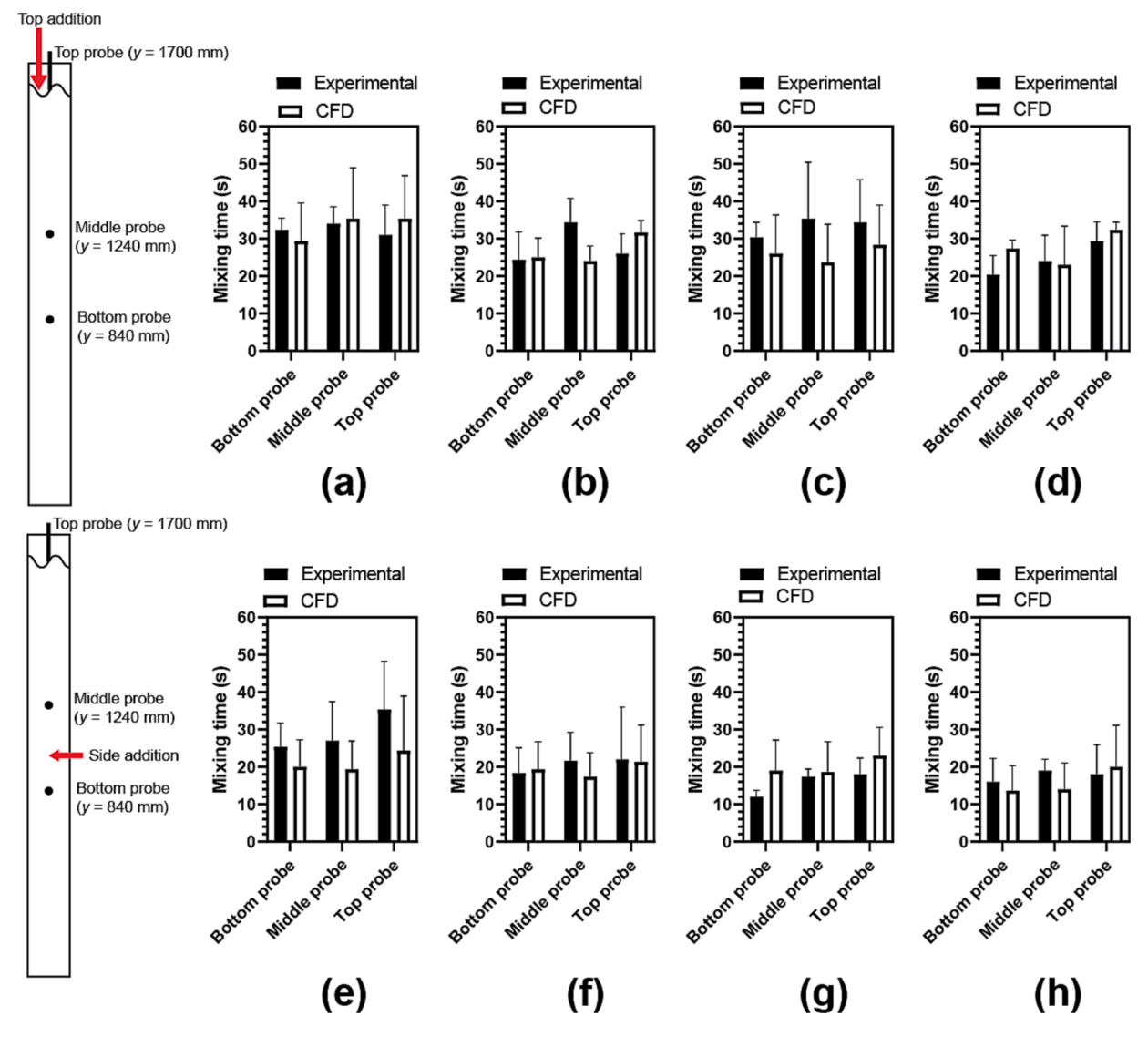


Fig. 5. Comparison between experimentally measured values of the mixing time and CFD predictions. Results are shown for two tracer addition locations and three measurement locations. All results are the average of three tracer additions, with error bars denoting one standard deviation about the mean. Results on the top row (a)-(d) are for tracer addition to the top of the column, results on the bottom row (e)-(h) are for tracer addition in the middle of the column. The first column (a) and (e) are for a superficial velocity of 0.6 cm s⁻¹, the second column (b) and (f) are for a superficial velocity of 1.6 cm s⁻¹, the third column (c) and (g) is for a superficial velocity of 3.2 cm s⁻¹ and the last column (d) and (h) are for a superficial velocity of 6.0 cm s⁻¹.

initial bubble sizes between 9 and 19 mm for the superficial velocities examined in this work. This, combined with the experimental measurements is consistent with the idea that the bubbles produced by the sparger undergo break-up as they rise through the column.

Fig. 6 gives a comparison between the experimentally measured mixing times and those predicted by the CFD model. Both the experimental measurements and CFD predictions showed a considerable amount of variation, this is due to the transient nature of the flow inside the bubble column, where the instantaneous flow pattern at the time of tracer addition impacts upon the mixing time [39]. Generally speaking, the model predictions were in good agreement with the experimental measurements for the range of superficial velocities $(0.6-6.0~{\rm cm~s}^{-1})$ and tracer addition and measurement locations examined. It was observed that increasing the superficial velocity led to a reduction in the mixing time, as expected, with the measured values being less than those predicted $(46-108~{\rm s})$ using correlations from the literature [54,55]. Interestingly, it was found that the measurement location did not have a large impact on the mixing time with the values being similar for the three points examined. However, it was found that the tracer addition

location did have an impact on the mixing time, with the side addition point generally resulting in lower mixing times than when the tracer was introduced to the top of the column, the reduction being of the order 40–80 %. This can be most likely be explained by the fact that when the tracer is added to the top of the column it has to travel a greater distance to be uniformly mixed throughout the column, thereby resulting in a longer mixing time.

As shown in Figs. 3-5 the CFD model offers a good prediction of the hydrodynamics within the bubble column, at a range of superficial velocities and measurement locations. Hence, the CFD model is suitable to be used as a basis for quantifying photobioreactor performance.

3.2. Validation of modelling workflow

The next step in the model validation process was to compare the predictions of the cell growth generated by the model workflow with experimental data. This comparison is given in Fig. 6 for *P. tricornutum*. It was found that the model was in good agreement with the experimental predictions, demonstrating that the workflow developed was

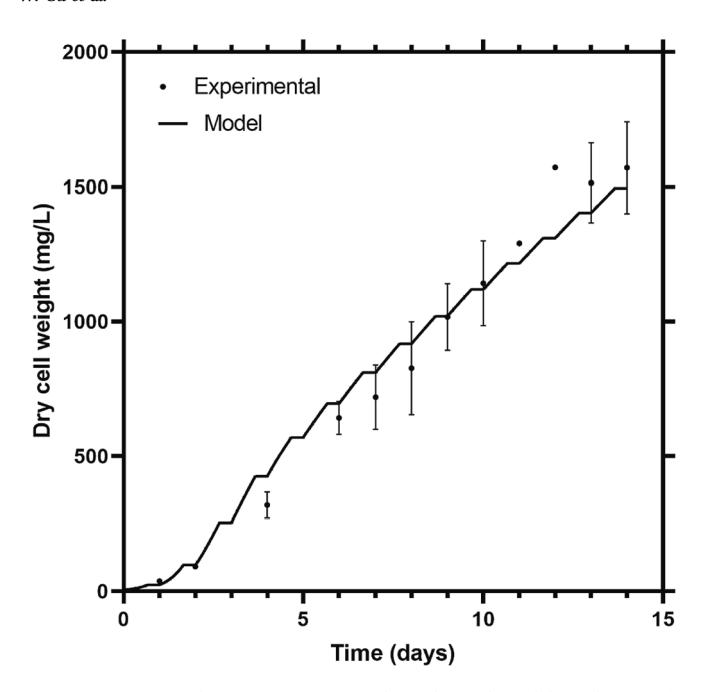


Fig. 6. Comparison between experimental results and model predictions for growth of *P. tricornutum* in 50 L bubble column bioreactors. Experiments were performed at a superficial velocity of $1.3~\rm cm~s^{-1}$; the same conditions were used in the modelling. Results are shown for three runs, with error bars denoting one standard deviation about the mean.

able to offer predictions in line with experimental measurements.

To further understand the model behaviour, plots of the calculated light field for cell densities from 250 to 1500 mg $\rm L^{-1}$ were generated and are shown in Fig. 7. As expected the illumination within the photobioreactor is not uniform due to the fact that light is being provided from three sides of the reactor. Similarly, it can be observed that the central portion of the reactor is essentially 'dark', while the edges are illuminated, and that the size of the dark zone increases with cell density (due to greater attenuation of the light). These results demonstrate that the best way to improve the growth of the algal culture would be to ensure cells are not 'trapped' in the central, 'dark' area of the column.

As part of the model validation the sensitivity of the model to various input parameters was examined. Unsurprisingly, the chosen value of the attenuation coefficient (K_a) had a large impact on the model predictions, with this effect being most pronounced as the culture density increased (i.e., towards the end of the batch). Our previous work [46] had shown that the value of K_a changed depending on the availability of nitrate, and the chosen value (0.35 L mg⁻¹ m⁻¹) was representative of conditions from day 5 onwards. In this work we have used the Beer-Lambert law to model light attenuation; this approach being selected on the basis of its simplicity. However, it may be desirable to replace this approach with a more complex model of light attenuation [56,57], something which can be done in a relatively straightforward manner using the current workflow. Similarly, it may be desirable to consider wavelength dependent behaviour when modelling absorption and scattering within the culture. Such an approach would introduce considerable additional complexity to the model. Given it was possible to achieve good agreement between the model predictions and experimental results (see Fig. 6) without accounting for wavelength dependent behaviour it remains an open question as to whether the increase in model accuracy justifies the additional complexity.

3.3. Evaluation of alternative PBR designs and operating conditions

Previous work [58] using a PBR of similar size showed that increasing the superficial velocity led to increased biomass productivity

for P. tricornutum. It was hypothesized that the improvement in productivity at higher superficial velocities was due to an increase in the L/D frequency. However, this was not experimentally quantified, as previously noted making such measurements is very challenging. By using the modelling approach developed in this work we are able to quantify the effect of the superficial velocity on the L/D cycle frequency, and hence the growth of the cultures.

Fig. 8 shows the effect of the superficial velocity on the predicted performance of the bubble column PBR. It was found that increasing the superficial velocity led to an improvement in the predicted biomass concentration, particularly for a superficial velocity of 6 cm s^{-1} . Increasing the superficial velocity will lead to an increase in the liquid velocity within the column, and hence improved mixing (as shown in Fig. 5). This will also lead to the cells being transported more rapidly between the column walls (i.e., the 'light' portion of the PBR) and the centre of the column (the 'dark' portion of the PBR). Such behaviour is observed in Fig. 8, where increasing the superficial velocity leads to an increase in the L/D cycle frequency, the average light intensity and hence the average specific growth rate. The predicted biomass productivity at a superficial velocity of 6 cm s⁻¹ was 144 mg L⁻¹ day⁻¹, this being approximately 40 % higher than the value at 1.6 cm s⁻¹ (104 mg L^{-1} day⁻¹). These results are in line with previously published results [58] for a similar PBR design growing P. tricornutum. Based on these results increasing the superficial velocity may be an easy way to improve the performance of the PBR. However, there are two potential drawbacks to this approach. Firstly, there is the obvious increase in energy required to supply the higher flow rate of air. Secondly, the increase in superficial velocity may lead to damage to the cells [58] which would obviously make this approach unfeasible. An advantage of the modelling approach developed here is that it is possible to quantify the trade-off between the increase in biomass concentration and energy demand, allowing systematic process design and optimisation.

As previously noted, a range of authors have reported that modifying the PBR design to include baffles or other internal structures led to increases in the biomass productivity [18–22]. Such increases were again attributed to increased mixing along the light gradient, which led to an increase in the L/D cycle frequency and in turn an improvement in the biomass productivity. Using the modelling workflow developed here it is possible to systematically evaluate new PBR designs *in silico* to determine their performance.

Fig. 9 shows the predicted performance for a range of PBR designs. Of the configurations examined it was found that the airlift and disc and donut baffles were predicted to give improved performance, while including the alternating baffles worsened the performance. Interestingly, the alternating baffles were also predicted to increase the light—dark cycle frequency, something which is thought to lead to improved performance. However, this configuration also led to a substantial reduction in the average light intensity experienced by the cells (Fig. 9 (c)). This is caused by the flow 'confining' the cells in the central portion of the column, away from the illuminated surface. Preliminary experimental work (shown in Supplementary Fig. S7) indicated that the model predictions agreed with the experimental data, with the performance of the column with the alternating baffles being similar to or worse than the standard bubble column without any internals.

Of the configurations evaluated the disc and donut baffles were predicted to offer the most improved performance, with the predicted biomass productivity being 145 mg $\rm L^{-1}$ day $^{-1}$, this being an approximately 40 % improvement when compared with the bubble column without internals. Interestingly, the airlift configuration offered a similar increase in performance, while not improving the light–dark cycle frequency to the same extent. This may be explained by the fact that the baffle in the airlift confines the cells closer to the walls of the PBR where they are more likely to experience a higher light intensity. These results highlight the potential advantages of installing internals in PBRs, as they can lead to substantially improved performance. However, this must also be weighed against any increases in capital cost, as well as

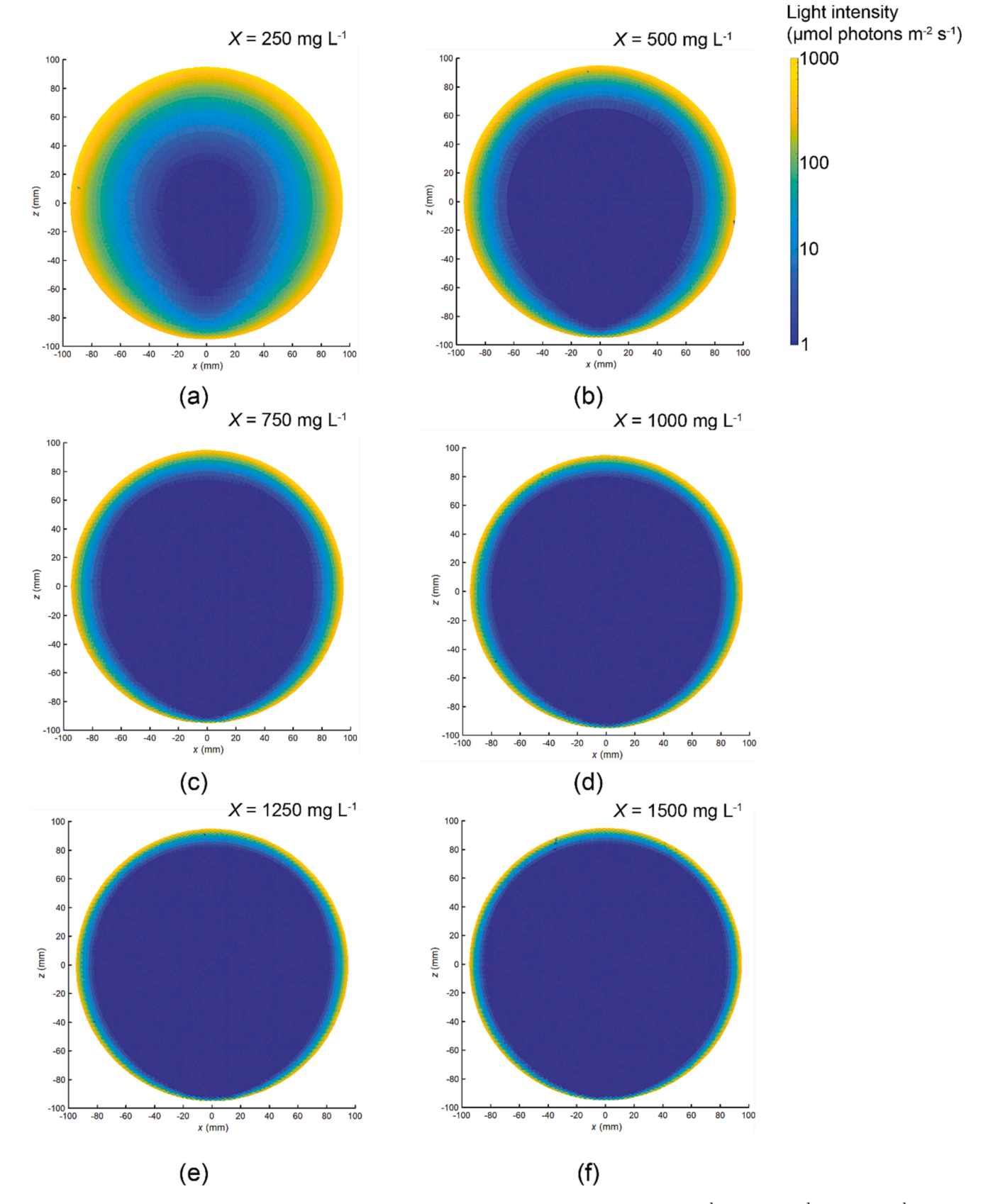


Fig. 7. Plot showing calculated light profiles in the PBR. Values have been calculated at cell densities of (a) 250 mg L^{-1} , (b) 500 mg L^{-1} , (c) 750 mg L^{-1} , (d) 1000 mg L^{-1} , (e) 1250 mg L^{-1} and (f) 1500 mg L^{-1} .

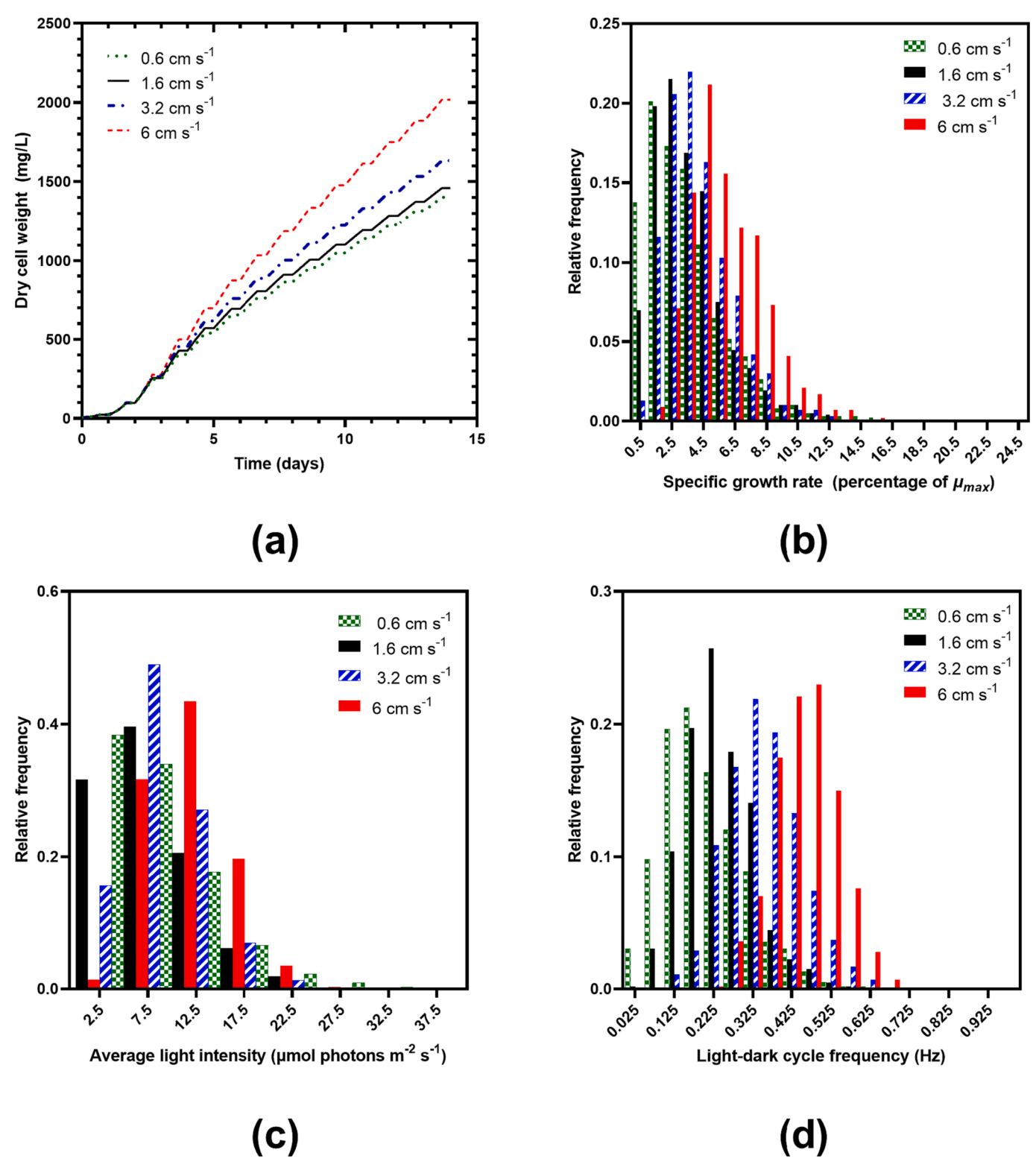


Fig. 8. Plots showing the effect of the superficial velocity on the performance of the PBR. (a) shows the effect of the superficial velocity on the predicted dry cell weight for the course of the cultivation. Plots (b), (c) and (d) have been calculated for a fixed cell density of 1500 mg L⁻¹ and show the distribution of the specific growth rate (b), the time-averaged light intensity (c), and the light-dark cycle frequency (d) for the population of particles.

any additional operational challenges (e.g., making cleaning more difficult).

The results shown in Fig. 9 suggest that the key metric in optimising the system is the average light intensity experienced by the cells, and that the light–dark cycle frequency cannot be considered in isolation.

These results also show the advantage of the approach developed in

this work, as it is possible to simultaneously evaluate multiple designs *insilico*. To illustrate this point, each algal cultivation performed in this work took approximately two weeks, with an additional 1–2 days being needed for cleaning and set-up of the PBRs. In the same amount of time it was possible to perform all of the CFD simulations used in this work in parallel. This demonstrates that once the model has been set-up and

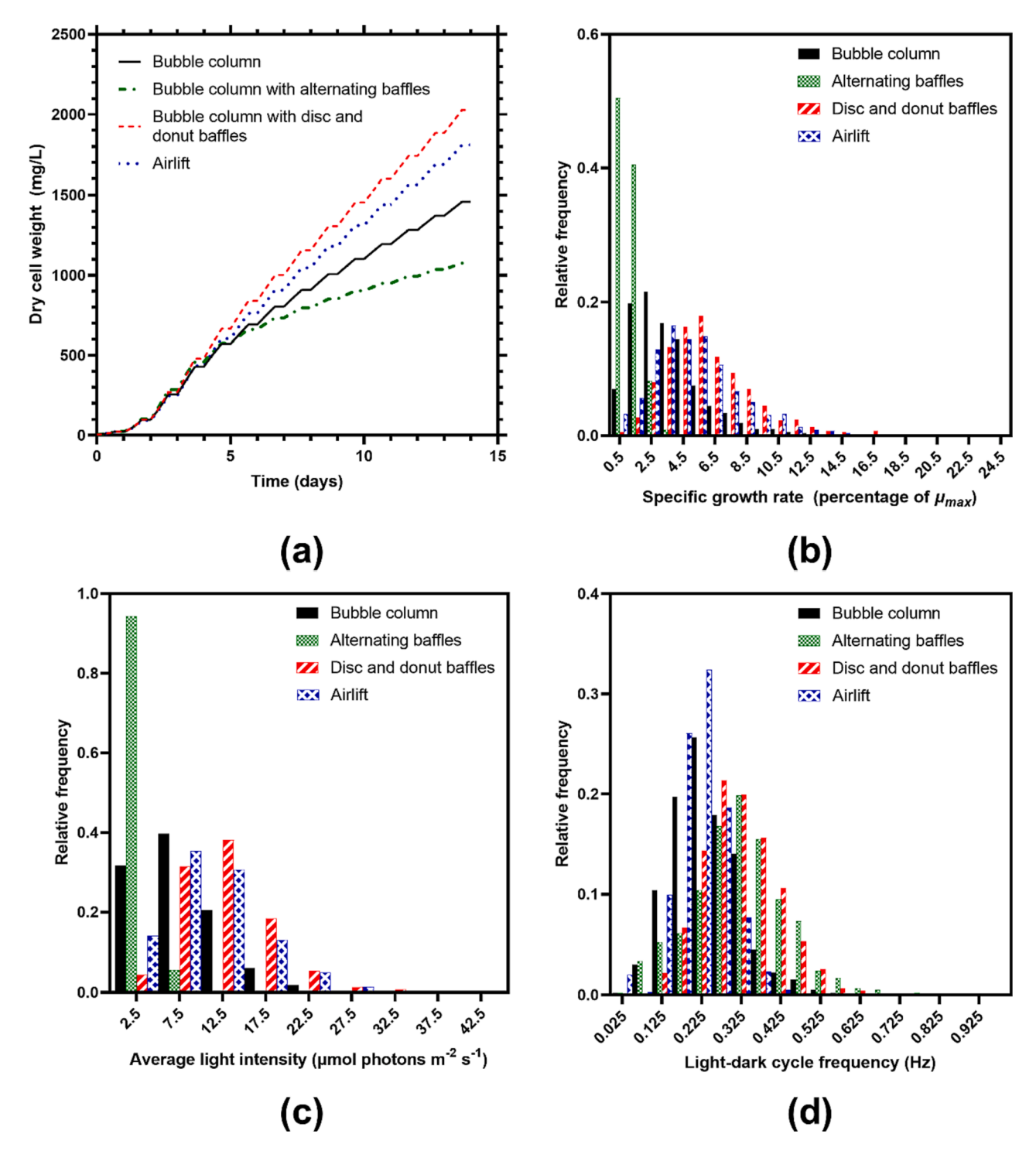


Fig. 9. Plot showing the effect of changing the PBR design on its performance. The predicted growth curves are shown in (a), while plot (b) shows the distribution of the specific growth rate for the modelled particle population, (c) shows the time-averaged light intensity and (d) shows the light–dark cycle frequency. Plots (b), (c) and (d) have been calculated for a cell density of 1500 mg L⁻¹. All simulations were performed at a superficial velocity of 1.6 cm s⁻¹.

validated it can be used to examine a range of conditions, with the aim of identifying the most promising for experimental evaluation.

4. Conclusions

In this work we have developed and validated a modelling approach which synthesises CFD, Monte-Carlo modelling and kinetic models to enable the detailed characterisation of PBR performance. The approach developed in this work enables the effect of different reactor designs and

operating conditions to be characterised throughout the course of an entire batch. This enables *in-silico* evaluation of different reactor configurations, potentially reducing the time and risk involved in the scale-up process.

The CFD model used in this work was based on our previous research into models for bubble column bioreactors [38,40] and in this work we have extensively validated it against experimental data across the range of superficial velocities likely to be used in bubble column PBRs. Results from the CFD were then combined with illumination and kinetic models

to develop a workflow which can be used to characterise the effect of different reactor designs and operating conditions. It was found that the model predictions were in good agreement with the experimental data for the widely cultivated diatom P. tricornutum. Using the model, it was possible to evaluate the effect of different reactor designs and operating conditions. For example, increasing the superficial velocity from 1.6 cm s⁻¹ to 6 cm s⁻¹ was predicted to lead to an approximately 40 % increase in the biomass productivity. The model can also be used to examine a range of different internal designs, it was found that some designs led to worse performance, while others were predicted to improve the biomass productivity. Of the configurations examined, the disc and donut baffles were predicted to increase the biomass productivity by a factor of approximately 40 % at a superficial velocity of 1.6 cm s⁻¹. Interestingly, it was found the key metric in the reactor design was the average light intensity experienced by the cells, and not the light/dark cycle frequency.

An advantage of the modelling approach used in this work is that can be readily extended to model any reactor design, an obvious area for future work would be to evaluate additional alternative internal configurations and then experimentally test the most promising. The aim of this work would be to increase the cell density/biomass productivity of photoautotrophic systems, a key factor in the overall process economics. Development of a reliable, accurate *in silico* method for screening reactor designs could potentially considerably simplify the photobioreactor design process, thereby facilitating scale-up. Similarly, being able to predict the performance of different reactor designs would be useful in performing techno-economic analyses.

An advantage of the workflow developed here is that it is possible to change the sub-models in a relatively straightforward way. For example, the model of light attenuation could be modified to be wavelength dependent, without requiring changes in the CFD or growth models. Potential further avenues for investigation could include looking at the growth of other species, as well as modifying the light model to be representative of sunlight in order to model outdoor cultures.

In conclusion, the approach outlined here can be used for the comprehensive characterisation of PBR performance and hence the development of optimised designs. This is a topic of considerable importance in increasing the productivity of photoautotrophic production systems and thereby enabling their wider deployment.

Declaration of Competing Interest

The authors declare that they have no known competing financial interests or personal relationships that could have appeared to influence the work reported in this paper.

Data availability

Data has been uploaded to the repository here: 10.17633/rd. brunel.23905842

Acknowledgements

The authors acknowledge the Sydney Informatics Hub and the University of Sydney's high-performance computing cluster, Artemis, for providing the computing resources that have contributed to the results reported herein.

Appendix A. Supplementary data

Supplementary data to this article can be found online at https://doi.org/10.1016/j.cej.2023.147032.

References

- M.A. Borowitzka, High-value products from microalgae—their development and commercialisation, J. Appl. Phycol. 25 (3) (2013) 743–756.
- [2] Y. Chisti, Biodiesel from microalgae, Biotechnol. Adv. 25 (3) (2007) 294–306, https://doi.org/10.1016/j.biotechadv.2007.02.001.
- [3] N.J. Oliver, C.A. Rabinovitch-Deere, A.L. Carroll, N.E. Nozzi, A.E. Case, S. Atsumi, Cyanobacterial metabolic engineering for biofuel and chemical production, Current Opinion in Chemical Biology 35(Supplement C) (2016) 43-50. https://doi. org/https://doi.org/10.1016/j.cbpa.2016.08.023.
- [4] M.J. Barbosa, M. Janssen, C. Südfeld, S. D'Adamo, R.H. Wijffels, Hypes, hopes, and the way forward for microalgal biotechnology, Trends Biotechnol. 41 (3) (2023) 452–471, https://doi.org/10.1016/j.tibtech.2022.12.017.
- [5] C. Posten, Design principles of photo-bioreactors for cultivation of microalgae, Eng. Life Sci. 9 (3) (2009) 165–177, https://doi.org/10.1002/elsc.200900003.
- [6] M. Janssen, Chapter Four Microalgal Photosynthesis and Growth in Mass Culture, in: L. Jack (Ed.), Advances in Chemical Engineering, Academic Press, 2016, pp. 185–256
- [7] P.S.C. Schulze, R. Guerra, H. Pereira, L.M. Schüler, J.C.S. Varela, Flashing LEDs for Microalgal Production, Trends Biotechnol. 35 (11) (2017) 1088–1101, https://doi. org/10.1016/j.tibtech.2017.07.011.
- [8] L.S. Sabri, A.J. Sultan, M.H. Al-Dahhan, Split internal-loop photobioreactor for Scenedesmus sp. microalgae: Culturing and hydrodynamics, Chin. J. Chem. Eng. (2020), https://doi.org/10.1016/j.cjche.2020.07.058.
- [9] L.S. Sabri, A.J. Sultan, M.H. Al-Dahhan, Investigating the cross-sectional gas holdup distribution in a split internal-loop photobioreactor during microalgae culturing using a sophisticated computed tomography (CT) technique, Chem. Eng. Res. Des. 149 (2019) 13–33, https://doi.org/10.1016/j.cherd.2019.06.017.
- [10] K.L. Terry, Photosynthesis in modulated light: Quantitative dependence of photosynthetic enhancement on flashing rate, Biotechnol. Bioeng. 28 (7) (1986) 988–995, https://doi.org/10.1002/bit.260280709.
- [11] M. Yoshioka, T. Yago, Y. Yoshie-Stark, H. Arakawa, T. Morinaga, Effect of high frequency of intermittent light on the growth and fatty acid profile of Isochrysis galbana, Aquaculture 338 (2012) 111–117.
- [12] C. Vejrazka, M. Janssen, M. Streefland, R.H. Wijffels, Photosynthetic efficiency of Chlamydomonas reinhardtii in flashing light, Biotechnol. Bioeng. 108 (12) (2011) 2905–2913, https://doi.org/10.1002/bit.23270.
- [13] M. Janssen, L. de Bresser, T. Baijens, J. Tramper, L.R. Mur, J.F.H. Snel, R. H. Wijffels, Scale-up aspects of photobioreactors: effects of mixing-induced light/dark cycles, J. Appl. Phycol. 12 (3) (2000) 225–237, https://doi.org/10.1023/A: 1008151526680.
- [14] P.C. Schulze, C. Brindley, J.M. Fernandez, R. Rautenberger, H. Pereira, R. H. Wijffels, V. Kiron, Flashing light does not improve photosynthetic performance and growth of green microalgae, Bioresource Technology Reports (2019), 100367, https://doi.org/10.1016/j.biteb.2019.100367.
- [15] C. Combe, P. Hartmann, S. Rabouille, A. Talec, O. Bernard, A. Sciandra, Long-term adaptive response to high-frequency light signals in the unicellular photosynthetic eukaryote Dunaliella salina, Biotechnol. Bioeng. 112 (6) (2015) 1111–1121, https://doi.org/10.1002/bit.25526.
- [16] E. Sforza, D. Simionato, G.M. Giacometti, A. Bertucco, T. Morosinotto, Adjusted Light and Dark Cycles Can Optimize Photosynthetic Efficiency in Algae Growing in Photobioreactors, PLoS One 7 (6) (2012) e38975.
- [17] H. Takache, J. Pruvost, H. Marec, Investigation of light/dark cycles effects on the photosynthetic growth of Chlamydomonas reinhardtii in conditions representative of photobioreactor cultivation, Algal Res. 8 (2015) 192–204, https://doi.org/ 10.1016/j.algal.2015.02.009.
- [18] J. Degen, A. Uebele, A. Retze, U. Schmid-Staiger, W. Trösch, A novel airlift photobioreactor with baffles for improved light utilization through the flashing light effect, J. Biotechnol. 92 (2) (2001) 89–94.
- [19] L.-L. Wang, Y. Tao, X.-Z. Mao, A novel flat plate algal bioreactor with horizontal baffles: structural optimization and cultivation performance, Bioresour. Technol. 164 (2014) 20–27.
- [20] J. Huang, Y. Li, M. Wan, Y. Yan, F. Feng, X. Qu, J. Wang, G. Shen, W. Li, J. Fan, Novel flat-plate photobioreactors for microalgae cultivation with special mixers to promote mixing along the light gradient, Bioresour. Technol. 159 (2014) 8–16.
- [21] J. Huang, F. Feng, M. Wan, J. Ying, Y. Li, X. Qu, R. Pan, G. Shen, W. Li, Improving performance of flat-plate photobioreactors by installation of novel internal mixers optimized with computational fluid dynamics, Bioresour. Technol. 182 (2015) 151–159.
- [22] Z. Yang, J. Cheng, X. Xu, J. Zhou, K. Cen, Enhanced solution velocity between dark and light areas with horizontal tubes and triangular prism baffles to improve microalgal growth in a flat-panel photo-bioreactor, Bioresour. Technol. 211 (2016) 519–526, https://doi.org/10.1016/j.biortech.2016.03.145.
- [23] H.J. Ryu, K.K. Oh, Y.S. Kim, Optimization of the influential factors for the improvement of CO2 utilization efficiency and CO2 mass transfer rate, J. Ind. Eng. Chem. 15 (4) (2009) 471–475, https://doi.org/10.1016/j.jiec.2008.12.012.
- [24] J.C. Merchuk, M. Gluz, I. Mukmenev, Comparison of photobioreactors for cultivation of the red microalga porphyridium sp, J. Chem. Technol. Biotechnol.: Int. Res. Process Environ. Clean Technol. 75 (12) (2000) 1119–1126.
- [25] G. Nadal-Rey, D.D. McClure, J.M. Kavanagh, S. Cornelissen, D.F. Fletcher, K. V. Gernaey, Understanding gradients in industrial bioreactors, Biotechnol. Adv. 46 (2021), 107660, https://doi.org/10.1016/j.biotechadv.2020.107660.
- [26] J.P. Bitog, I.B. Lee, C.G. Lee, K.S. Kim, H.S. Hwang, S.W. Hong, I.H. Seo, K.S. Kwon, E. Mostafa, Application of computational fluid dynamics for modeling and designing photobioreactors for microalgae production: A review, Comput.

- Electron. Agric. 76 (2) (2011) 131–147, https://doi.org/10.1016/j.compag.2011.01.015.
- [27] B.A. Cho, R.W.M. Pott, The development of a thermosiphon photobioreactor and analysis using Computational Fluid Dynamics (CFD), Chem. Eng. J. 363 (2019) 141–154, https://doi.org/10.1016/j.cej.2019.01.104.
- [28] C. McHardy, G. Luzi, C. Lindenberger, J.R. Agudo, A. Delgado, C. Rauh, Numerical analysis of the effects of air on light distribution in a bubble column photobioreactor, Algal Res. 31 (2018) 311–325, https://doi.org/10.1016/j. algal.2018.02.016.
- [29] P. Ranganathan, A.K. Pandey, R. Sirohi, A. Tuan Hoang, S.-H. Kim, Recent advances in computational fluid dynamics (CFD) modelling of photobioreactors: Design and applications, Bioresource Technology 350 (2022) 126920. https://doi. org/https://doi.org/10.1016/j.biortech.2022.126920.
- [30] J.C.M. Pires, M.C.M. Alvim-Ferraz, F.G. Martins, Photobioreactor design for microalgae production through computational fluid dynamics: A review, Renew. Sustain. Energy Rev. 79 (2017) 248–254, https://doi.org/10.1016/j. resr 2017.05.064
- [31] G. Luzi, C. McHardy, C. Lindenberger, C. Rauh, A. Delgado, Comparison between different strategies for the realization of flashing-light effects – Pneumatic mixing and flashing illumination, Algal Res. 38 (2019), 101404, https://doi.org/10.1016/ i.elgal. 2018.104464
- [32] R. Laifa, J. Morchain, L. Barna, P. Guiraud, A numerical framework to predict the performances of a tubular photobioreactor from operating and sunlight conditions, Algal Res. 60 (2021), 102550, https://doi.org/10.1016/j.algal.2021.102550.
- [33] L. Li, Z.M.H. Mohd Shafie, T. Huang, R. Lau, C.-H. Wang, Multiphysics simulations of concentric-tube internal loop airlift photobioreactors for microalgae cultivation, Chemical Engineering Journal 457 (2023), 141342, https://doi.org/10.1016/j. cei.2023.141342.
- [34] E. Ertekin, J.M. Kavanagh, D.F. Fletcher, D.D. McClure, Validation studies to assist in the development of scale and system independent CFD models for industrial bubble columns, Chem. Eng. Res. Des. 171 (2021) 1–12, https://doi.org/10.1016/ i.cherd.2021.04.023.
- [35] G. Nadal-Rey, J.M. Kavanagh, B. Cassells, S. Cornelissen, D.F. Fletcher, K. V. Gernaey, D.D. McClure, Modelling of industrial-scale bioreactors using the particle lifeline approach, Biochem. Eng. J. 198 (2023), 108989, https://doi.org/10.1016/j.bej.2023.108989.
- [36] D.D. McClure, J.M. Kavanagh, D.F. Fletcher, G.W. Barton, Development of a CFD model of bubble column bioreactors: part one a detailed experimental study, Chem. Eng. Technol. 36 (12) (2013) 2065–2070, https://doi.org/10.1002/ceat.201300544
- [37] W. Liu, N.N. Clark, A.I. Karamavruç, Relationship between bubble size distributions and chord-length distribution in heterogeneously bubbling systems, Chem. Eng. Sci. 53 (6) (1998) 1267–1276, https://doi.org/10.1016/S0009-2509 (97)00426-0
- [38] D.D. McClure, H. Norris, J.M. Kavanagh, D.F. Fletcher, G.W. Barton, Validation of a Computationally efficient computational fluid dynamics (CFD) model for industrial bubble column bioreactors, Ind. Eng. Chem. Res. 53 (37) (2014) 14526–14543, https://doi.org/10.1021/ie501105m
- [39] D.D. McClure, N. Aboudha, J.M. Kavanagh, D.F. Fletcher, G.W. Barton, Mixing in bubble column reactors: experimental study and CFD modeling, Chem. Eng. J. 264 (2015) 291–301, https://doi.org/10.1016/j.cej.2014.11.090.
- [40] D.F. Fletcher, D.D. McClure, J.M. Kavanagh, G.W. Barton, CFD simulation of industrial bubble columns: Numerical challenges and model validation successes, App. Math. Model. 44 (2017) 25–42, https://doi.org/10.1016/j.apm.2016.08.033.
- [41] R. Clift, J.R. Grace, M.E. Weber, Bubbles, Academic Press, New York, Drops and Particles. 1978.

- [42] D.D. McClure, J.M. Kavanagh, D.F. Fletcher, G.W. Barton, Experimental investigation into the drag volume fraction correction term for gas-liquid bubbly flows, Chem. Eng. Sci. 170 (2017) 91–97, https://doi.org/10.1016/j. cos. 2016.12.066
- [43] A.D. Burns, T. Frank, I. Hamill, J.-M. Shi, The Favre Averaged Drag Model for Turbulent Dispersion in Eulerian Multi-Phase Flows, 5th International Conference on Multiphase Flow, Yokohama, Japan, 2004.
- [44] W. Yao, C. Morel, Volumetric interfacial area prediction in upward bubbly twophase flow, Int. J. Heat Mass Transf. 47 (2) (2004) 307–328, https://doi.org/ 10.1016/j.ijheatmasstransfer.2003.06.004.
- [45] Ansys, CFX User's Manual, 2021.
- [46] W. Gu, J.M. Kavanagh, D.D. McClure, A scalable model for EPA and fatty acid production by Phaeodactylum tricornutum, Front. Bioeng. Biotechnol. 10 (2022), https://doi.org/10.3389/fbioe.2022.1011570.
- [47] E. Marken, N. Ssebiyonga, J.K. Lotsberg, J.J. Stamnes, B. Hamre, Ø. Frette, A. S. Kristoffersen, S.R. Erga, Measurement and modeling of volume scattering functions for phytoplankton from Norwegian coastal waters, J. Mar. Res. 75 (5) (2017) 579–603, https://doi.org/10.1357/002224017822109514.
- [48] A. San Pedro, C.V. González-López, F.G. Acién, E. Molina-Grima, Marine microalgae selection and culture conditions optimization for biodiesel production, Bioresource Technology 134 (2013) 353–361, https://doi.org/10.1016/j. biortech.2013.02.032.
- [49] K.L. Terry, J. Hirata, E.A. Laws, Light-limited growth of two strains of the marine diatom Phaeodactylum tricornutum Bohlin: Chemical composition, carbon partitioning and the diel periodicity of physiological processes, J. Exp. Mar. Biol. Ecol. 68 (3) (1983) 209–227, https://doi.org/10.1016/0022-0981(83)90054-0.
- [50] V. Patil, T. Källqvist, E. Olsen, G. Vogt, H.R. Gislerød, Fatty acid composition of 12 microalgae for possible use in aquaculture feed, Aquac. Int. 15 (1) (2006) 1–9, https://doi.org/10.1007/s10499-006-9060-3.
- [51] W. Gu, J.M. Kavanagh, D.D. McClure, Photoautotrophic production of eicosapentaenoic acid, Crit. Rev. Biotechnol. (2021) 1–18, https://doi.org/ 10.1080/07388551.2021.1888065.
- [52] S. Kim, Y.-J. Jung, O.-N. Kwon, K. Cha, B.-H. Um, D. Chung, C.-H. Pan, A potential commercial source of fucoxanthin extracted from the microalga phaeodactylum tricornutum, Appl. Biochem. Biotechnol. 166 (7) (2012) 1843–1855, https://doi. org/10.1007/s12010-012-9602-2.
- [53] K. Akita, F. Yoshida, Bubble size, interfacial area, and liquid-phase mass transfer coefficient in bubble columns, Ind. Eng. Chem. Process Des. Dev. 13 (1) (1974) 84–91, https://doi.org/10.1021/i260049a016.
- [54] Y. Kawase, M. Moo-Young, Mixing time in bioreactors, J. Chem. Technol. Biotechnol. 44 (1) (1989) 63–75, https://doi.org/10.1002/jctb.280440107.
- [55] J. Tramper, K. van't Riet, Basic Bioreactor Design, M, Dekker, New York, 1991.
- [56] Y.S. Yun, J. Park, Attenuation of monochromatic and polychromatic lights in Chlorella vulgaris suspensions, Appl. Microbiol. Biotechnol. 55 (6) (2001) 765–770. https://doi.org/10.1007/s002530100639.
- [57] J.F. Cornet, C.G. Dussap, G. Dubertret, A structured model for simulation of cultures of the cyanobacterium Spirulina platensis in photobioreactors: I. coupling between light transfer and growth kinetics, Biotechnol. Bioeng. 40 (7) (1992) 817–825, https://doi.org/10.1002/bit.260400709.
- [58] A.S. Mirón, M.C.C. García, A.C. Gómez, F.G.a. Camacho, E.M. Grima, Y. Chisti, Shear stress tolerance and biochemical characterization of Phaeodactylum tricornutum in quasi steady-state continuous culture in outdoor photobioreactors, Biochemical Engineering Journal 16(3) (2003) 287-297. https://doi.org/https:// doi.org/10.1016/S1369-703X(03)00072-X.